



Division of Informatics, University of Edinburgh

Institute of Perception, Action and Behaviour

Artificial ears for a biomimetic sonarhead: from multiple reflectors to surfaces

by

DaeEun Kim, John Hallam, Nico Kaempchen, Jose Carmena

Informatics Research Report EDI-INF-RR-0061

Division of Informatics
<http://www.informatics.ed.ac.uk/>

April 2001

Artificial ears for a biomimetic sonarhead: from multiple reflectors to surfaces

DaeEun Kim, John Hallam, Nico Kaempchen, Jose Carmena

Informatics Research Report EDI-INF-RR-0061

DIVISION *of* INFORMATICS

Institute of Perception, Action and Behaviour

April 2001

Artificial Life 7:2, pp. 147-169, MIT Press.

Abstract :

This work presents an evolutionary approach to pinna design. Narrowband echolocating bats move the pinna to alter the directional sensitivity of their perceptual systems. Adding pinnae to RoBat — a biomimetic sonarhead mounted on a mobile robot — is the goal of this work. After a description of the earlier work on artificial pinnae consisting of multiple reflectors around the transducer, an acoustic model, inspired by a physical model of sound diffraction and reflections in the human concha, is described and revisited as the model to use for evolving complex shapes. A genetic algorithm evolved the shape of the pinnae with respect to desired features of the directivity pattern of the receiver transducers. Some interesting paraboloid shapes for specific echolocating behaviours were evolved, improving performance with respect to the bare transducer's performance.

Keywords : pinna, genetic algorithm, echolocation, sonar, bat, robot

Copyright © 2002 by The MIT Press.

The authors and the University of Edinburgh retain the right to reproduce and publish this paper for non-commercial purposes.

Permission is granted for this report to be reproduced by others for non-commercial purposes as long as this copyright notice is reprinted in full in any reproduction. Applications to make other use of the material should be addressed in the first instance to Copyright Permissions, Division of Informatics, The University of Edinburgh, 80 South Bridge, Edinburgh EH1 1HN, Scotland.

Artificial ears for a biomimetic sonarhead: from multiple reflectors to surfaces

J.M. Carmena*, N. Kämpchen, D. Kim and J.C.T. Hallam
Institute of Perception, Action and Behaviour
Division of Informatics, University of Edinburgh
5 Forrest Hill, EH1 2QL, Scotland, UK

Abstract

This work presents an evolutionary approach to pinna design. Narrowband echolocating bats move the pinna to alter the directional sensitivity of their perceptual systems. Adding pinnae to RoBat — a biomimetic sonarhead mounted on a mobile robot — is the goal of this work. After a description of the earlier work on artificial pinnae consisting of multiple reflectors around the transducer, an acoustic model, inspired by a physical model of sound diffraction and reflections in the human concha, is described and revisited as the model to use for evolving complex shapes. A genetic algorithm evolved the shape of the pinnae with respect to desired features of the directivity pattern of the receiver transducers. Some interesting paraboloid shapes for specific echolocating behaviours were evolved, improving performance with respect to the bare transducer's performance.

1 Introduction

Bats exhibit navigation and prey-capture skills that when duplicated in a robot would be the envy of any robotics engineer. All the neural computations needed to perform the estimation tasks underlying the acquisition of vital information about the environment occur within a brain the size of a large pearl [27]. Stimulus ensembles on which these tasks have to be carried out range from simple single-target situations (e.g. track an insect in mid-air) to structure-rich environments, where each echo is a superposition of reflections from many reflecting facets.

One of the most obvious aspects of echolocating behavior is dynamics: bats are mobile animals; they often echolocate on the wing and can move their heads and pinnae as well as the nose or mouth whenever they emit echolocation signals. Narrowband echolocators move the pinna — a cartilageous flap of the external ear which is very mobile and has a highly convoluted surface in many bat species — to alter the directional sensitivity of their perceptual systems whereas broadband listening systems (e.g. humans and broadband emitting bats) rely on pinna *morphology* to alter acoustic directionality at different frequencies [30].

Biologists have investigated the importance in narrowband echolocating bats of pinna motion along vertical arcs for target localization in the vertical plane [6, 24]. This has been shown to be necessary for determining target elevation in *Rhinolophus ferrumequinum* [12]. It has even been hypothesised that this might explain their unusually large pinnae compared to the size of their head, as seen in Fig. 1.

*E-mail: jose@dai.ed.ac.uk

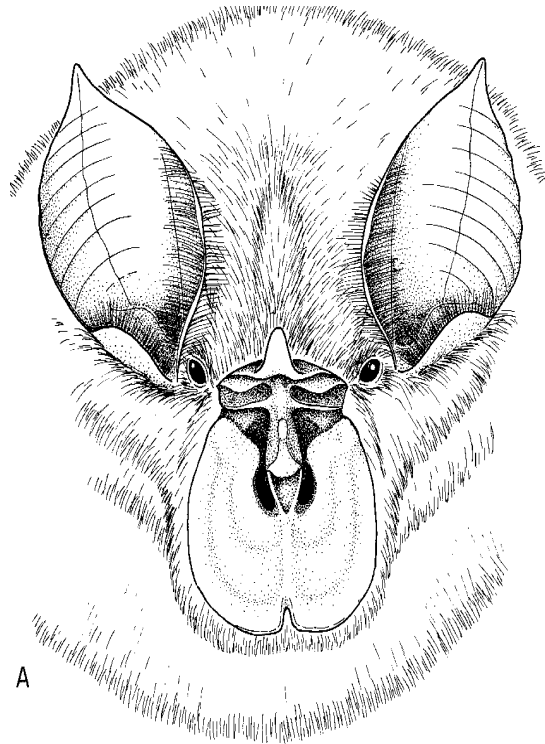


Figure 1: Drawing of *Rhinolophus ferrumequinum*. (Copyright by Dr. Martin Trappe)

The relationship between bats and robots arises because the sensor interpretation problems of bats, while navigating in cluttered environments such as forests, are very similar to those of mobile robots provided with ultrasonic sensors when navigating in laboratories. Moreover, the constant frequency part of the call emitted by the narrowband bats when echolocating is analogous to the one typically emitted by robotic ultrasonic sensors in terms of bandwidth.

1.1 RoBat: a biomimetic platform to study perception in bats

The RoBat project aims to investigate bat biosonar as a biological approach to mobile robot navigation, *i.e.* tries to understand how echolocating bats perform navigation tasks such as obstacle avoidance and prey capture, and how can this be applied to navigation in mobile robots [4].

RoBat consists of three main components: a biomimetic sonarhead (described below), a 3 DOF mobile platform and a signal processing package whose operations, performed upon the received echoes, are based upon a filterbank model of the processing performed by the mammalian cochlea [26]. These three components are all controlled and integrated into a single system by software running on a Pentium III PC (Linux).

The 6 DOF sonarhead, as indicated in Fig. 2 (left), allows panning and tilting of the neck, and independent panning and tilting of each of the two ears (receivers). The ultrasonic transducers are Polaroid electrostatic transducers. The motors driving the different axes are standard radio-control servomotors [19].

This setup when mounted on the mobile platform (Fig. 2 (right)) allowsinsonification of arbitrary points in space, independent of the orientation of the mobile platform. Taken together with the capability of the sonarhead to independently orient the ears it allows us to model different strategies that might be used by bats to actively explore their

environment [18].

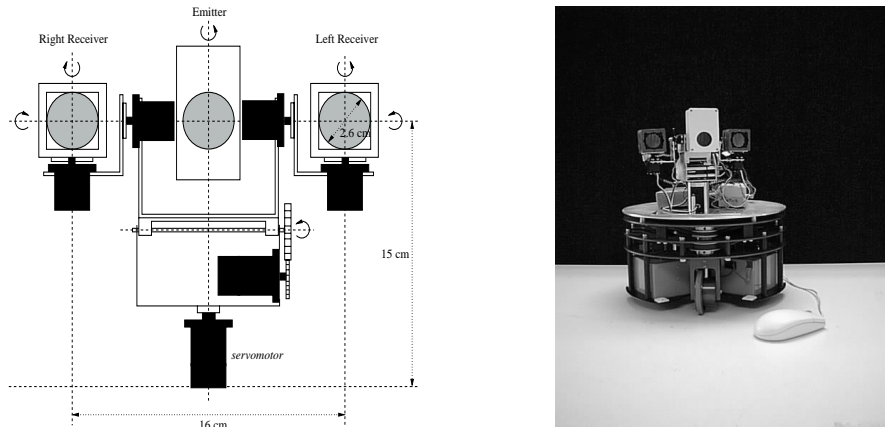


Figure 2: Front view of the sonarhead consisting of the central emitter fixed to the head and the two receivers each independently orientable (left). RoBat, a biomimetic sonarhead mounted on a mobile platform. (right).

The goals of creating a tool such as RoBat are twofold. It will help engineers to better understand the relationships existing between environment features and their corresponding acoustic images in a dynamic context. Such a tool seems necessary as apart from work on prosthetic devices for the blind [7] and work on convolution-based ultrasonic sensors [17, 9], most research on ultrasonic sensors for mobile robots has suffered from the ‘ultrasonic sensor = Polaroid range sensor’ fallacy. This sensor [2], by extracting Time-Of-Flight (TOF) for the first echo only, discards most of the information present in the echo signal. Hence extensive post-processing has to be performed on large numbers of range readings to construct consistent and reliable environment models [13, 10] out of them. From the study of biological acoustic sensorimotor systems [23, 14], however, we conclude that much more information can be extracted from these echoes. Doing so leads to improved robotic ultrasonic sensors [20].

At the same time, such a tool will also help biologists studying echolocation in bats better to understand what type of information is available to the bat while performing particular tasks. Biologists are becoming interested in such tools as this robotics approach to biology allows them to explore the sensory world of animals with synthetic observers and test hypotheses for adaptive sensing behaviour in real-world conditions [30]. Hence, a physical model, *i.e.* a robotic implementation, of an acoustic sensorimotor system complements the more traditional mathematical models. From the merger of these two disciplines, biology and robotics, biorobotics arises. We define biomimetic sensing systems as man-made systems which implement functional principles of their biological counterparts, either as a research tool for biology or as an engineering application. Biomimetic systems do not violate any of the known constraints on biological function, but forgo replicating any detail of biological structure irrelevant to the problem under study.

Thus, as part of our working plan, we pursue improvement of the directional sensitivity of the sonarhead’s receivers (*i.e.* maximise the angular resolution of the receiving transducers), as well as the echo amplitude, by adding artificial pinnae to them. As a result of this increased discrimination, echolocating behaviours such as arc scanning and interaural intensity differences (which we will see in next section) could be replicated in the sonarhead more successfully than using only bare transducers.

Next, some relevant concepts about bats are introduced (section 2). Then, a review of previous work on artificial pinnae (Section 3) is presented as well as a description of the revision of the acoustic model used in our previous work (Section 4). The genetic algorithm used for evolving surfaces is described in Section 5. Then, different experiments are designed and their results discussed (Section 6). Finally, the conclusions of this work are given in Section 7.

2 Background on bats

Bats can be divided into two broad non-taxonomic groups based on the time-frequency-structure of their echolocation pulses: For FM bats (FM = frequency modulated), such as the Big Brown Bat *Eptesicus fuscus*, echolocation calls are multi-harmonic chirps. Duration and bandwidth of the frequency sweep as well as the shape of the instantaneous frequency as a function of time vary between species. The frequency range covered extends up to approximately 200 kHz. In CF-FM bats, echolocation pulses are often dominated by prolonged CF (=constant frequency) signal portions, although frequency-modulated “tails” are always present as well. Allocation of energy to the CF and FM portions of a signal varies with behavioral context [28]. Well known species of CF-FM bats are the Greater Horseshoe Bat *Rhinolophus ferrumequinum* and the Mustached Bat *Pteronotus parnellii*.

The bat’s auditory system is structured in the same way as that of other mammals (see, e.g., [22]). The incident sound is directed towards the ear canal by the pinna, a cartilaginous flap of the external ear, which is very mobile and has a highly convoluted surface in many bat species. The transduction stage located in the inner ear (cochlea) performs a joint time-frequency analysis of the incoming signal. A simple model of this analysis is a bandpass filter bank with subsequent demodulation in each channel by a combination of half-wave rectification and lowpass filtering. In the FM bats the layout of the auditory filter bank follows the general mammalian pattern of keeping filter quality constant as center frequency varies. CF-FM bats deviate considerably from this pattern by forming an auditory fovea in the frequency range where the carrier frequencies of the echoes are kept by the Doppler-shift compensation behavior of these animals [1]. Towards the center of the fovea, filter qualities rise steeply to the highest values known (maximum $Q_{10dB} \sim 400$ in *Rhinolophus ferrumequinum*); outside this frequency band the CF-FM bats follow the general mammalian pattern.

It is quite interesting to see the way in which echolocators with narrow-band call structures perform target localisation. In the case of the CF-FM bat, this localisation is performed mostly using the information contained in a single harmonic echo. In order to calculate the target’s azimuth angle with a receiver placed on each side of the head (as in bats), interaural intensity differences (IIDs) as well as interaural time differences (ITDs) can be employed.

However, how can the elevation angle be estimated? Earlier experiments with the biomimetic sonarhead [30] showed how, by sweeping the receivers through opposite vertical arcs, dynamic cues, in the form of amplitude modulations which vary systematically with target elevation, are indeed created, suggesting at least one possible source of information the bats could use. From her results, Walker suggested that “if neurons exist to represent moving targets — as measured by stationary pinnae — then the apparent motion of a stationary target — as measured by moving pinnae — may be similarly encoded” [29]. Thus, arc scanning, combined with azimuth angle estimation by means of IIDs and target’s range by the echo delay, provides a narrow-band echolocator with a 3D estimation of an insonified target’s relative position.

3 Previous work on artificial pinnae

First attempts in evolving bat pinna morphology [16, 21] used genetic algorithms (GAs) to evolve simple pinna shapes for broadband echolocators because of the difficulty of designing a pinna model by an analytical approach. The evolved solutions were evaluated on a software model of the biomimetic sonarhead described above [29].

The pinna was modelled by up to three disc reflectors whose position and orientation angle around the receiving transducer were determined by a GA, using a chromosome with the following structure,

$$(x_1 \ y_1 \ z_1 \ \alpha_1 \ \beta_1 \quad x_2 \ y_2 \ z_2 \ \alpha_2 \ \beta_2 \quad \dots \quad x_n \ y_n \ z_n \ \alpha_n \ \beta_n)$$

where x, y and z are cartesian position coordinates and α, β are azimuth and elevation angles. The GA comprised a population of candidate sets of reflector positions, whose fitness was determined by simulating their effect on the acoustic signals transduced by the receiver. *2-point* crossover and a mutation rate of 0.03 were used with a population of 100. A tournament-selection scheme of size 8 wherein a set of genomes is randomly selected from the population was used. The fittest genome in the set was chosen with a given probability; if not selected, then the second best is selected with the same probability, and so on. Experiments were run for 1000 generations.

The GA in [21] was set two tasks: first, to deploy reflectors in a monaural system so as to maximise the displacement between the axes of maximal sensitivity at 30 kHz and 90 kHz (thereby allowing target elevation to be most accurately inferred from the different amplitudes of the echo at these frequencies); and second, to deploy reflectors in a binaural system to produce a maximally steep IID curve with respect to target angular position (thereby maximising the angular resolution of the binaural system and allowing the target's position to be most accurately estimated from the IID). In the binaural case, the left ear was symmetrical with the right ear, *i.e.* the two pinna configurations were derived from the single disposition of reflectors indicated by the GA. The results for the first experiment were reasonable, but for the second experiment no significant improvement of the IID performance could be obtained with up to three reflectors.

Such work was continued by us [8], changing the model to the narrowband (CF-FM bat) case and allowing up to 10 reflectors to be used by the GA. However, experiments with such a number of reflectors showed problems with phase cancellation in the received echoes. Also, diffraction and diffusion phenomena around the edges of the reflector discs were considered insignificant and no multiple reflections were taken into account, *i.e.* each reflector introduced one additional echo path. The necessity of a more realistic model of wave propagation which could be applied to complex surfaces therefore arose. An acoustic model inspired by a physical model of sound diffraction and reflections in the human concha [11], was the next step taken [5]. Such a model will be described next.

3.1 Computing reflections from finite reflectors

If we assume that the echo source is in the far field of the transducer and reflector system, the incoming echo will have planar wavefronts. (The near field case can be modelled similarly, with different assumptions about the incident waves.) The incident sound insonifies the transducer and reflectors, generating a pressure at each point \vec{r} on their surfaces which is given by

$$p_0(\vec{r}, t) = p_0 e^{j(\vec{k} \cdot \vec{r} - \omega t)} \quad (1)$$

where \vec{k} is the wave vector of the incident wave.

The total sound pressure field at the transducer is given by the direct path field, given by the equation above, and by the contributions from the reflectors. The reflector

contributions can be calculated using Kirchhoff's diffraction theory [3] — each point on the reflector surface is taken to be an acoustic source radiating sound in all directions. The sound pressure on any surface element of the transducer is then the integral of the contributions from each surface element of the reflector system. Using the diffraction theory model allows us to take account of the finite size of the reflector.

The reflected pressure generated at a point by a surface element on a reflector depends on the incident sound pressure, the distance to the point and the angle between the surface normal and the direction to the point. The relationship is defined by

$$dP_R(\vec{p}, t) = \frac{R(d, \gamma_0)p_0(\vec{r})}{d} e^{jkd - j\omega t} ds, \quad (2)$$

where $p_0(\vec{r}, t)$ is the incident sound pressure at position \vec{r} on the reflector surface (where the element ds is), d is the distance from the reflector surface element ds to the transducer (that is, $\|\vec{p} - \vec{r}\|$), k is the magnitude of the wave vector (that is, $\frac{2\pi}{\lambda}$ for a wave with wavelength λ) and γ_0 is the angle between the surface normal at \vec{r} and the line joining the surface element to the point \vec{p} for which the pressure is being calculated.

The directional factor for reflection is given by the reflector obliquity function [11]:

$$R(r, \gamma_0) = \frac{\cos\gamma_0}{4\pi} \left(-jk + \frac{1}{r}\right). \quad (3)$$

Therefore, integrating over the whole transducer surface S_T and the whole reflector surface S_R , we can obtain the total pressure contributed to the transducer which is given by the equation:

$$P_T = \iint_{S_T} \iint_{S_R} \frac{R(\|\vec{r} - \vec{p}\|, \gamma_0)p_0(\vec{r})}{\|\vec{r} - \vec{p}\|} e^{jk\|\vec{r} - \vec{p}\| - j\omega t} ds_r ds_t \quad (4)$$

A diagram of the plane wave model used for a transducer and reflector system is shown in Fig. 3 (left). In the figure, a plane wave arriving at a surface element \vec{r} of the reflector (R) insonifies a surface element \vec{p} of the transducer (T) along path $\vec{p} - \vec{r}$. Note, however, that each of the reflector's surface elements will behave as an acoustic source radiating sound in all directions, not only along $\vec{p} - \vec{r}$, as explained above.

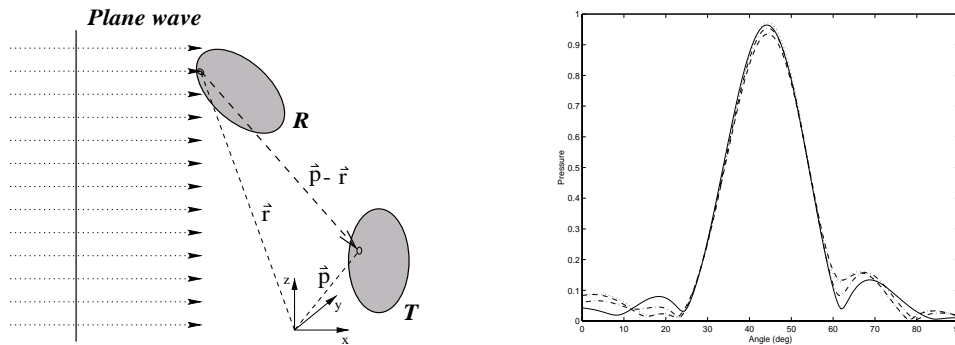


Figure 3: Left: Plane wave model with a single reflector (R) and a transducer (T). Right: 3D pressure vs. 800 div. reflector's effect on transducer for different angles (distances: 0.5 cm (solid), 0.75 cm (dashdot), 1 cm (dashed)); 2000 div. reflector at 1 cm (dotted).

For the sake of simplicity the model was applied numerically instead of analytically. The reflector and transducer surface pressures were calculated as the sum of contributions of finite elements (FE) as an approximation to the surface integral. The division into elements was calculated using polar coordinates, varying the radius and angle according

to the number of desired surface segments. Since the larger the number of divisions, the more accurate the calculation is, 2000 vs. 800 divisions were tested, resulting in a not very significant difference as seen in the overlapping dotted curve in Fig. 3 (right). Hence for the rest of the experiments 800 divisions were used.

Also, as evidence of plausibility of the simulation work, a coarse evaluation of the acoustic model in the real world was performed experimenting with one single reflector (Fig. 4 left). The receiver to which the reflector was attached was turned 90 degrees (facing the ceiling). In such a position, the bare receiver is not insonified by the echo and, therefore, a better estimation of the reflector’s effect can be obtained. Measurements were taken in increments of 7.5 degrees (from 90 to 0 degrees) with an estimated error of ± 1 degree along yaw (α) and pitch (β) angles. With respect to Cartesian coordinates a positioning error of ± 1 mm was assumed. For each measurement, 1000 consecutive pulses were sent by the emitter to a post located 30 cm in front of RoBat. The mean value of the echo energy was calculated for each of the pulses. As seen in Fig. 4 (left), the reflector’s vertical distance with respect to the transducer is 1 cm because of the gap between the transducer and the grid covering it.

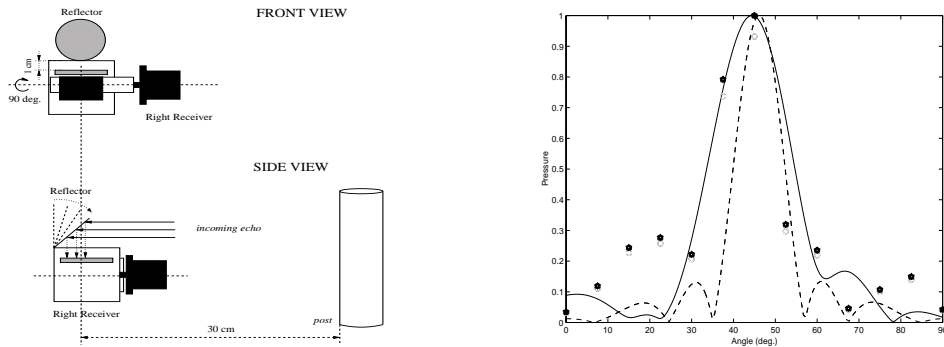


Figure 4: Left: Experimental set-up for one reflector. Right: Results comparison between simulation work (previous model (dashed) and plane wave model (solid)) and real world (blobs).

Figure 4 (right) shows a comparison between simulation and real echo amplitude. In the figure, the solid line represents the plane wave model, the dashed line represents the previous model [21] and the blobs represent the mean of 1000 echo energy values. When the real measurements were taken, the physics of the transducer-reflector configuration was not as simple as the model described in Section 4. As can be seen in Fig. 2, each of the transducers is inside a square box covered by a grid¹. Some of the effects of this modified model can be appreciated in the interval between 10 and 30 degrees (Fig. 4 (right)) as a pressure offset value with respect to the simulated data. Another factor is the very low standard deviation (whose maximum value is 0.0042 in the scale of Fig. 4) obtained from the 13 sets (from 0 to 90 degrees in increments of 7.5) of 1000 samples. Thus, despite the physical differences of the real model, the data fitted encouragingly well for the preliminary experimental conditions in which the measurements were taken.

Figure 5 shows examples of 5 and 10 reflector configurations evolved by the GA for the current model. Because of the better results obtained, the model in [21] was replaced by the current model for further work in which spherical rather than point like waves are used.

¹This is to prevent accidental touching of the transducer (which is charged at 200 V) by the user’s fingers.

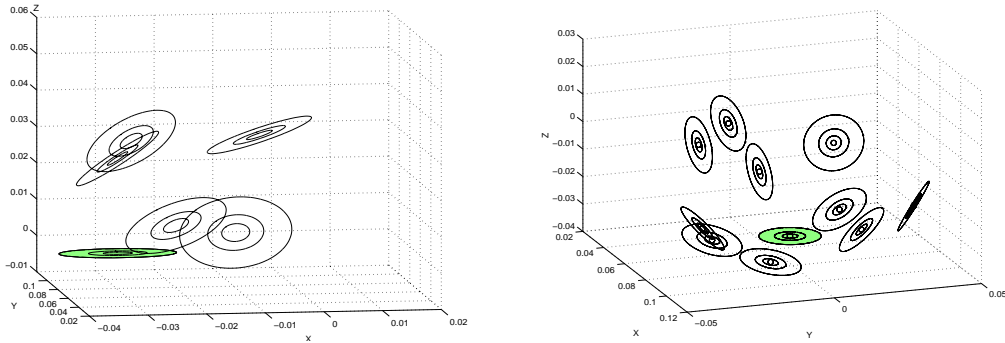


Figure 5: Evolved 5 (left) and 10 (right) reflector configurations around transducer (shadowed) using the plane wave model.

4 The acoustic model, revisited

In this section, a revision of the acoustic model described in previous section is done. This new version of the model suffices for a plausible design of more realistic pinna shapes.

For evolving the parameters of reflector shapes which optimise the echolocation task, the directivity and the IID map of the emitter-pinna-receiver combination must be taken into account. Therefore, the directivity must be calculated in order to evolve the reflector shapes in the simulator.

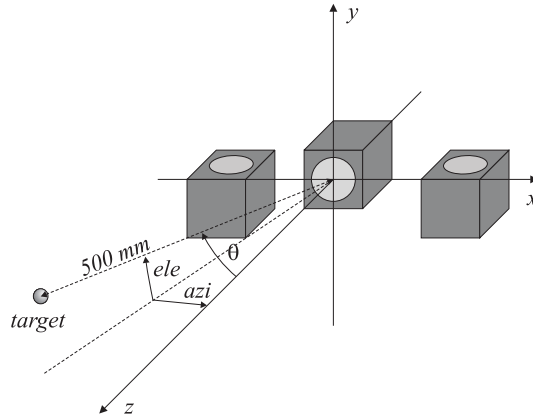


Figure 6: Global coordinate system

As seen in Section 1.1, in RoBat, sound is emitted by the transducer placed between the two “hearing” transducers of the sonarhead. The target is considered to be at a distance of 500 mm and has the insect-like shape of a small sphere (see Fig. 6). The amplitude of the sound wave arriving at the target depends on the target’s angular position relative to the sonarhead, as the emitter has a certain directivity. The echo is considered to be a plane wave when it is entering the two ears of the sonarhead

$$p(\vec{r}) = P_0 D(f, a, \theta) e^{j(\vec{k} \cdot \vec{r} - \omega t)}, \quad (5)$$

where \vec{k} is the wave vector and \vec{r} is the point of observation. $D(f, a, \theta)$ is the directivity of the emitter, defined as

$$D(f, a, \theta) = \frac{P(f, a, \theta)}{P(f, a, 0)}. \quad (6)$$

P_0 in Equation 5 is a constant and is set to 1 for the purpose of this work. The amplitude of the emitted sound wave as well as the attenuation effect of the reflected echo are considered to be constant as the target's range does not vary.

In order to calculate the directivity, the time course is not of interest, only the amplitude of the stationary sound wave. Therefore, a simplified version of Equation 5 is used to obtain the equation of the incident sound wave

$$p_i(\vec{r}) = P_0 D(f, a, \theta) e^{j\vec{k}\cdot\vec{r}}. \quad (7)$$

This sound wave enters the ear and is diffracted at the edges of the pinna aperture. The diffracted wave is then reflected by the pinna surface. The reflected sound waves produce a sound pressure on the transducer. Additionally the direct, unreflected echo applies pressure on the surface of the transducer if the transducer is not in the acoustic shadow of the reflector. The directivity of the system is given by the variation of pressure received by the transducer for different target positions.

A difficulty in the acoustic flow is the receiver box. As seen in Section 3, the transducer disc is situated 10 mm inside the box and covered by a plastic grid with holes of a diameter of 1.8 mm. For the continuation of this work, the grid was removed and the transducer was raised up to the same level as the side of the box².

In the physical model of the human concha not only reflection but also diffraction was considered [11]. In previous stages of this work [5] only reflection was taken into account. In order to decrease the significance of the diffraction on the resulting pressure on the transducer surface, the width and height of the aperture should be many wavelengths³. Assuming this condition, the wave inside the pinna, before hitting the reflector surface, can be approximated by the incident planar wave front as the diffracting component is small compared to the undisturbed sound wave.

4.1 Finite surface element model

In order to be able to calculate the resulting sound pressure on the transducer in Equation 4, the transducer as well as the reflector surface is divided into FE. The integration turns out to be a summation of finite pressure contributions which is easily calculated

$$P_w \simeq \sum \sum \left[p_i(\vec{r}_t) + \sum \sum p_i(\vec{r}_r) \frac{1}{2\pi l} \cos(\beta) \left(\frac{1}{l} - jk \right) e^{jk l} \Delta S_r \right] \Delta S_t. \quad (8)$$

The FE model used in earlier work [5], divides the transducer into parts which all have the same length in the radial direction and cover the same angle ($\Delta r = \text{constant}, \Delta \alpha = \text{constant}$). Therefore FE which are close to the edge of the transducer disc cover a larger area than those in the centre of the disc (see Fig. 7(a)), since

$$\Delta S_t \approx r \Delta r \Delta \alpha.$$

Therefore the FE near the centre are much smaller than those near the edge of the transducer disc. As the approximation in Equation 8 is only as good as the largest finite element, the elements near the centre become very small when good accuracy is needed in the approximation. In order to minimise the number of FE the transducer is here divided instead into FE of identical size. In the new model the length of both sides of the FE are kept constant. The length in the radial direction is constant for all elements as before. Conversely to the previous model, the length in angular direction is constant too

$$\Delta \text{step}_\alpha = r \Delta \alpha = \text{constant}. \quad (9)$$

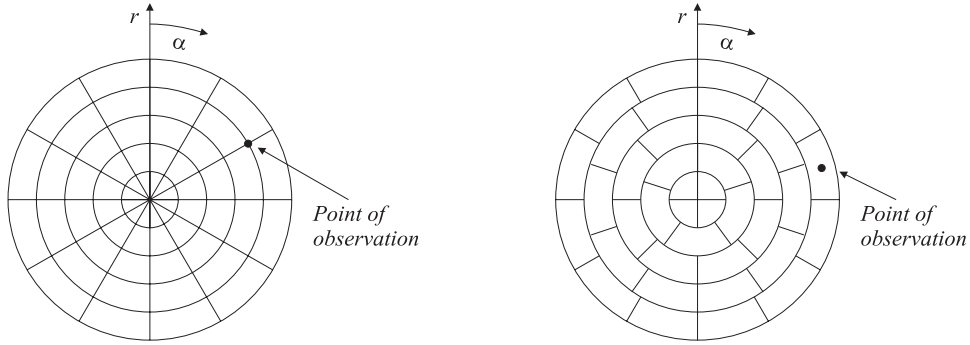


Figure 7: Old finite element model (left) and the new model with constant finite divisions (right).

Therefore the angle, but not the length in angular direction is different for different radii (see Fig. 7 (right)). The resulting area is constant for all FE

$$\Delta S_t \approx \Delta r \Delta step_\alpha = constant. \quad (10)$$

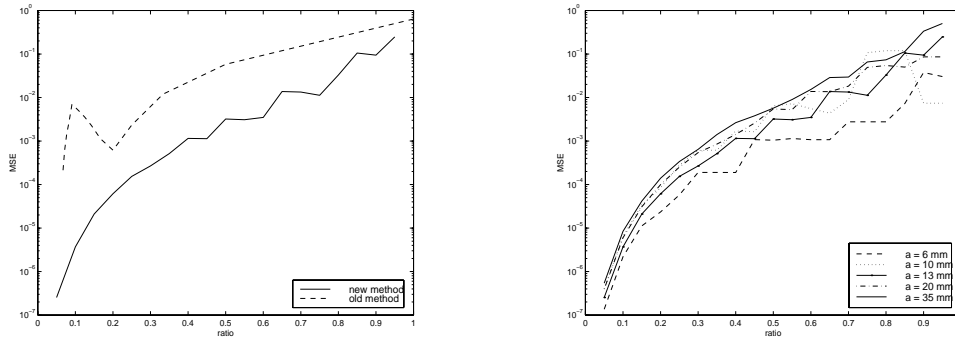


Figure 8: (Comparison between old and new finite element model (transducer radius $a = 13mm$) (left). Accuracy for different transducer radii and finite element sizes (right).

To increase the accuracy of the approximation, the point of observation is in the middle of the finite element, in contrast to the previous model where it was at one of the corners. In Figure 8 (left) the difference in accuracy between these two models is displayed. The accuracy is measured as the mean squared error (MSE) of the simulated directivity pattern of a bare transducer for several different lengths of FE. The error is obtained by comparing the simulated data with the analytical solution of the Polaroid transducer's Bessel function [17]. The ratio between the length of the finite element and the wavelength is shown on the x-axis

$$\Delta r = \Delta step_\alpha = ratio \times \lambda.$$

In addition to a higher accuracy the number of FE can be reduced by up to 50%, thus reducing computation time.

In Figure 8 (right) the accuracy of the new model is shown for different transducer disc sizes. For very small transducer radii and high ratios the model becomes unreliable.

²These changes were implemented into the simulator. However it is also possible to apply them to RoBat.

³The wavelength of the signal is $\lambda = 6.8mm (f = 50kHz)$.

However, this is not surprising, as the radius of $6mm$ is smaller than the wavelength of $\lambda = 6.8mm$ and therefore the transducer is divided into only a few FE for high ratios. As expected the MSE converges clearly towards zero, as the ratio becomes smaller and a good MSE is obtained for ratios under 0.4. The same principle applies for the reflector surface. However the mathematics to divide a conical or paraboloid shape into pieces of constant size is somewhat more complicated and only a tedious summation of equations.

This acoustic model has its limitations. It is only an approximation and has the disadvantage that the pressure contribution of a FE increases to infinity the nearer the point of observation is to the reflector surface (see Equation 8). It has been shown above that a high accuracy can be obtained for small FE sizes. It is, however, still necessary to investigate how close the transducer can be situated to the pinna.

5 From multiple reflectors to surfaces

Two reflector shapes are considered in this work, a conical and a paraboloid surface. Preliminary experiments on cylindrical shapes showed unfavourable results.

5.1 The conical external ear

The axis of the cone section coincides with the axis of the transducer and the radius of the cone gets smaller toward the top. The shape is open at the front where the angle of the aperture can be chosen. The surface is given by the equation

$$\left(\frac{x - c_x}{R}\right)^2 + \left(\frac{z - c_z}{R}\right)^2 = \frac{(h - y)^2}{h^2}. \quad (11)$$

In the parametric form a point on the reflector \vec{r}_r is given by

$$\vec{r}_r = \begin{pmatrix} x \\ y \\ z \end{pmatrix} = \begin{pmatrix} \frac{h-y}{h}R \sin(\alpha) + c_x \\ y \\ \frac{h-y}{h}R \cos(\alpha) + c_z \end{pmatrix}, \quad (12)$$

with the parameter $y \in [0, h]$.

The parameters which determine the shape of the cone are the radius R , height h , the displacement of the center c_x, c_z and the angle of the cone section γ .

The angular width γ determines the range of the parameter α

$$\pi - \frac{\gamma}{2} \leq \alpha \leq \pi + \frac{\gamma}{2}. \quad (13)$$

5.2 The paraboloid external ear

This reflector surface was chosen because of its amplifying characteristic. It is widely used to maximise the gain of a receiver in focusing the incoming waves to one point. Usually the paraboloid is obtained by rotating a parabola, so that a cut through the axis of the paraboloid is always a parabola and a cut orthogonal to the axis results in a circle. In this work a more general shape was chosen. The rotated parabola changes its steepness, so that a cut orthogonal to the axis results in an ellipse. The axis of the reflector is parallel to the z axis (see Fig. 9). The paraboloid is described by the cartesian equation

$$\left(\frac{x - c_x}{a}\right)^2 + \left(\frac{y}{b}\right)^2 - (z - c_z) = 0 \quad (14)$$

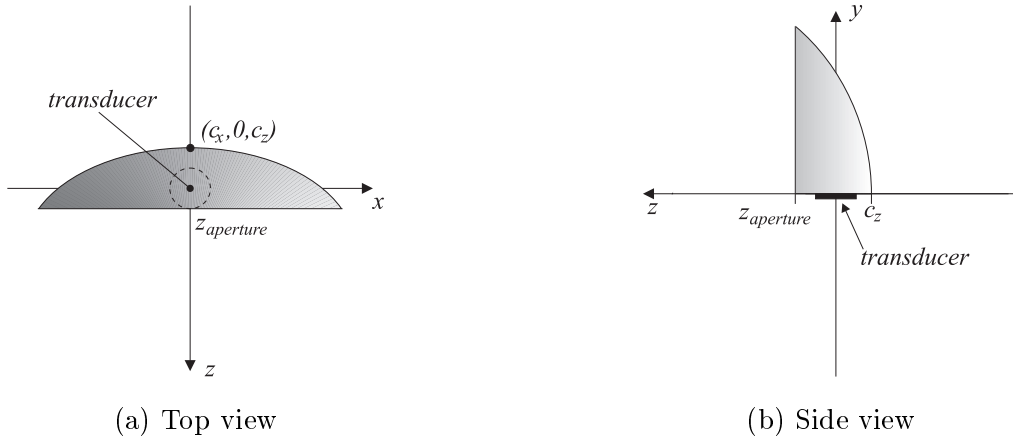


Figure 9: Parameters of the paraboloid shape

or by the parametric equations

$$\vec{r}_r = \begin{pmatrix} x \\ y \\ z \end{pmatrix} = \begin{pmatrix} \sqrt{u}a \sin(\alpha) + c_x \\ \sqrt{u}b \cos(\alpha) \\ u + c_z \end{pmatrix}, \quad (15)$$

with $u \in [0, z_{aperture} - c_z]$ and

$$-\frac{\pi}{2} \leq \alpha \leq \frac{\pi}{2}. \quad (16)$$

The parameters which determine the shape of the paraboloid are the radius in the x direction, a , the radius in the y direction, b , the displacement of the center c_x, c_z and the position of the aperture plane $z_{aperture}$ (see Fig. 9).

5.3 The Genetic Algorithm

5.3.1 Encoding the parameters

Both shapes are defined by five parameters. Of these five parameters, four were chosen for evolution since c_x — the displacement in x direction — was considered to be almost redundant because of the azimuthal orientation parameter of the receiver configuration. Together with the two angles of the orientation of the receivers there are six parameters to evolve. The position of the transducer boxes relative to the emitter were considered to be fixed and the distances were adopted from the sonarhead of RoBat.

These six parameters form a chromosome, in which each gene can take 21 different values, integers from 0 to 20, which are mapped to the real valued parameters by the linear transformation

$$parameter = factor \times gene + offset. \quad (17)$$

5.3.2 Crossover, mutation and selection

A simple one-point crossover is used with a probability of 1. The chromosomes of the parents are broken up randomly at the same point and the new child is formed by adding the first part from one parent to the second part of the other chromosome.

Each gene of the new chromosome is then mutated with the probability of 0.2. A gene is mutated by replacing it with a new random value. Mutation facilitates the search for new solutions and also agitates against a convergence of the population. The high

mutation rate of 0.2 was chosen empirically and is explained by a small population size of 50 chromosomes.

A tournament selection operator, in which several members of the population are randomly chosen, was used. Better chromosomes are preferred, repeating this process until finding the other parent. The tournament size regulates the selection pressure. The smaller the tournament is, the lower is the pressure for a chromosome to be fit in order to win the tournament. For this task a small tournament size of 2 was chosen, therefore reducing the fitness pressure and enabling diversity of chromosomes.

5.3.3 The fitness function

The fitness of a chromosome is a measurement of its quality. The quality in this case is determined by the performance of the reflector-transducer combination in the echolocation task. As mentioned in Section 2, the model bat in this work is the species called *Rhinolophus ferrumequinum*, a CF-FM bat which emits 83 kHz calls. The three fitness functions described next were used in this work.

Maximising the gain An important characteristic of the pinna is its gain. The gain is defined by the difference of the maximal sound pressure received with and without the added pinna

$$f_1 = 20 \log(\max(P_{pinna})) - 20 \log(\max(P_{transducer})), \quad (18)$$

and characterises the ability of the pinna to focus the received sound towards the transducer surface.

Vertical target localisation As shown in Fig. 10 (left) an ear movement strategy is adopted. However, instead of moving only the pinnae, the whole receiver configuration including the transducer performs arc scanning as described in Section 2. The movement is sinusoidal with an amplitude of 15° .

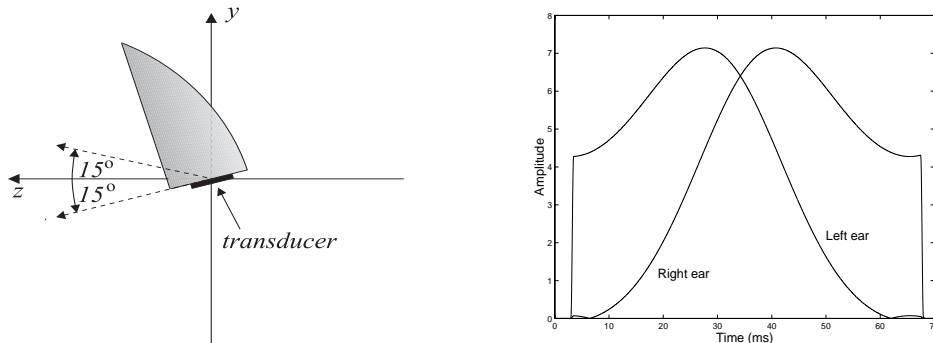


Figure 10: The pinna mounted on the transducer performing vertical arcs for elevation estimation (left). The delay between amplitude peaks encodes the target elevation — here for a sonarhead without pinnae and a target elevation of 6° (right).

To improve the accuracy of the elevation estimation the directivity of the ear should have a certain characteristic. Ideally it should be very sensitive in one direction and not at all in other directions. Thus only at a certain moment in the arc scanning process would an echo be received. In general, this can be formulated as a need to maximise the directionality in one direction and minimise the sensitivity in other elevations:

$$f_2 = \text{mean}(\text{peak}_{azi} - \max(\text{sidepeaks}_{azi})), \quad (19)$$

the average of the difference of the main sensitivity and the highest side sensitivity over different azimuths. If there are no side peaks, the minimal sound pressure is taken instead.

Horizontal target localisation As seen in Section 2, bats estimate the target’s azimuth angle from the IID. The question is which values from the arc scanning should be taken in order to calculate the IID. The approach chosen in this work was to take the highest value of one ear and the value of the other at the *same* position, as the resulting IID curve then depends only on the emitter directivity and not on the receiver directivity, which simplifies the target’s position estimation.

Once the values are found by arc scanning the difference is calculated in order to obtain the IID. The IID is given by the difference of the sound pressures between the left and right transducer:

$$IID = 20 \log \frac{P_r}{P_l} = 20(\log P_r - \log P_l). \quad (20)$$

As the IID depends on the target’s azimuth, the latter can be estimated. In Fig. 12 (right, dashed), the IID plotted for a sonarhead without pinnae for 0° elevation when performing arc scanning is shown. At least three parameters describe the quality of this curve:

1. The *steepness*, which determines the angular resolution. The steeper the IID is, the more accurately the target’s azimuth can be estimated.
2. The *range* from one peak to the other characterises the width of the acoustic field of view.
3. The *shape* of the curve. A linear IID simplifies the calculation of the target’s azimuth angle. On the other hand a sinusoidal or sigmoidal curve might be preferred. Both exhibit a high steepness and therefore high acuity at the center and less accuracy for larger angles. These shapes allow target azimuth estimations of higher quality if the target is in focus.

In all experiments a linear IID was sought by the GA. The range of the IID curve was determined by the first local optimum encountered if the search starts from 0° azimuth to the left and right. The steepness of the curve is the difference of pressure between the left and right peak. The linearity is determined by the mean squared error between the IID curve and a fitted line.

The sound pressure of the echo is dependent on the emitter directivity pattern. Therefore, the scope of view of the perception system is limited by the main lobe of the emitter if the emitter is static. Additionally, the intensity curve of the echo at a certain elevation changes for different elevation angles, as the main lobe of the emitter has different horizontal widths at different elevations.

Therefore, the drawback is that the field of view becomes more limited the more the target elevation differs from 0° if arc scanning is applied. Even if the IID is independent of the emitter directivity, the quality of the echolocation decreases drastically if the target’s solid angle is close to that of the notch around the emitter’s main lobe. The received echoes are so weak that they are overwhelmed by noise in the receiver system. A possibility for overcoming these disadvantages is to tilt the whole head, as the direction of the emitter’s main lobe then changes with the head motion. The field of view is therefore independent of the elevation.

Also, a possibility for overcoming too strong an IID dependence, other than by head movements, is to change the emitter. With a smaller emitter, the main lobe becomes wider and the dependence of the echo intensity on the target elevation insignificant. This approach would mimic the sound emission of natural bats [25]. The directivity of the nostrils of the *Rhinolophus ferrumequinum* is much more similar to the pattern of a transducer of 4 mm radius than of the one of 13 mm which is implemented in RoBat.

5.3.4 Performance of the GA

The GA was programmed in C as was the acoustic simulator. The PVM (parallel virtual machine) program and its libraries were used to run different fitness functions in parallel on up to 90 machines.

A steady state GA was chosen, which replaces one member of the population at a time by a new created child. As soon as the fitness of the child is calculated, a new chromosome is sent for evaluation. This guarantees that all machines, running in parallel, are always provided with chromosomes to be evaluated, which maximises efficiency. A side effect is that the evaluation takes place asynchronously. It can occur that a child is inserted into the population before another which was sent for evaluation first.

Two methods for replacing an old member of the population by a new chromosome are used.

1. *Crowding*. A child replaces the chromosome it is most similar to, if the fitness of the former is higher. This promotes high variety between the members of the population. Several (local) optima are approached at the same time. The drawback is that this search is very slow.
2. The *least-fit* member of the population is replaced if the fitness of the new chromosome is higher. This method aims for the best solution. The drawback is that the population converges fast towards one chromosome.

In the course of the evolution, first crowding is applied for 1000 replacements, followed by 2000 new children which are inserted by the least-fit operator. Therefore a parallel search for different optima is first performed whereas thereafter the evolution focuses on the most promising optimum. As it was not obvious whether the fitness function has one or several optima, the performance of the GA was adapted for both possibilities, *i.e.* the GA first considers all local optima and then focuses on one (hopefully the best). The parameters (described at the beginning of this section) were chosen empirically and the performance was satisfactory.

6 Results

First, investigations with the GA to maximise the gain of a pinna surface are presented. Then, a description of the performance of different shapes is given with respect to the echolocation task where the neck is moved in elevation. Some of the results obtained are also investigated in the last part of this section, where arc scanning is performed.

Each time the directivity of only the left ear is evolved. As the configuration is assumed to be symmetric, the directivity of the right ear is obtained by the mirror directivity pattern of the left ear. The mirror plane is the Z-Y plane.

6.1 Maximising the gain

The gain of a pinna-transducer configuration depends on two parameters: on the ability of the pinna to focus the incident sound wave on the transducer surface and on the transducer area. Smaller transducers receive less sound pressure than larger ones.

In the experiments the emitter always had a radius of 4 mm. The sound pressure is normalised to the sound pressure received by a 13 mm bare transducer which is perfectly directed towards the center of the emitter's main lobe.

The conical and paraboloid pinnae were evolved as well as the null position of the bare transducer. Two receiver disc sizes were used: 4 and 13 mm radius. This is summarised in the following table:

	max pressure with pinna (dB)	max pressure without pinna (dB)	gain (dB)
conical, 4 mm	-12.21	-20.46	8.25
paraboloid, 4 mm	1.10	-20.46	21.56
conical, 13 mm	-0.16	-0.03	-0.13
paraboloid, 13 mm	4.31	-0.03	4.34

Though the maximal amplitude is obtained by the paraboloid with a receiver disc radius of 13 mm, the best gain results from the combination of a paraboloid with the smaller transducer of 4 mm radius. The maximal sound pressure received by the 4 mm transducer is even higher than that measured by the much larger 13 mm transducer without pinna.

The maximal pressures received by the bare transducer of 13 mm were expected to be 0 dB, as the sound pressure was normalised by this configuration. The small difference of -0.03 dB can be explained by the granularity of the alignment. The angle of the null position could be chosen by the GA in 2° steps. Interestingly the null position of both bare transducer evolutions is at 0° elevation and 8° azimuth. Therefore the left ear is pointing towards the direction of targets which are in the center of the emitter's main lobe, in order to align its own main lobe with that of the emitter.

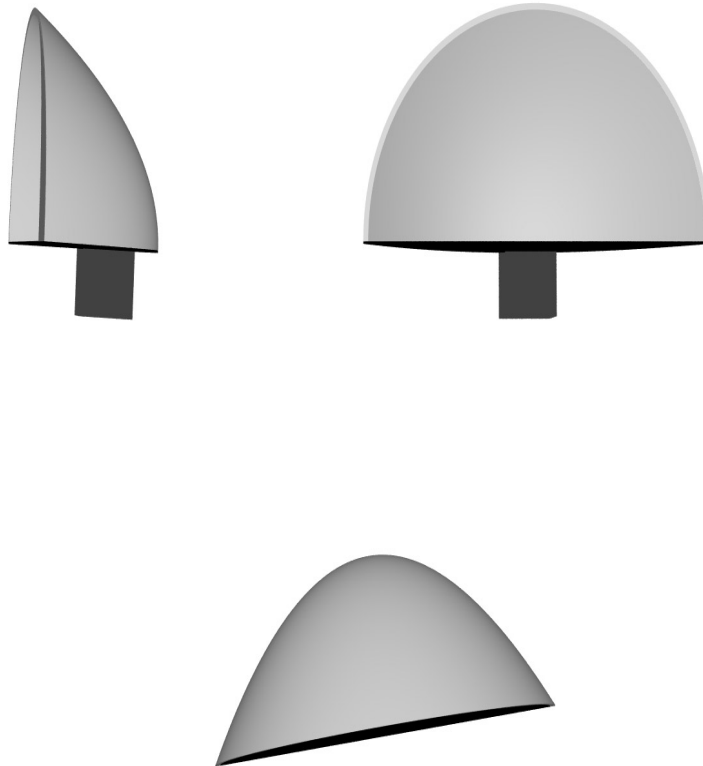


Figure 11: Paraboloid shape which maximises the gain to 21.56 dB.

In figure 11, the resulting paraboloid shape can be seen. The shape tried to expand in

the time course of the evolution and came to the size limit which was given by the setup of the GA.

6.2 Tilting the neck

The GA next evaluated shapes in order to improve a neck tilting task. The receivers together with the emitter perform a vertical rotation, which was assumed to be unlimited. The head is moved towards the direction where the loudest echo comes from and then oscillates around that direction in order to estimate the target's elevation. The azimuth is estimated by the IID of the loudest received echo throughout a period of head movement.

For a bare transducer without pinnae there is a tradeoff between the steepness and the broadness of the IID. If the broadness is enlarged the maximal values of the IID decrease and the curve becomes less steep. Additionally, the shape of the IID curve is fixed. It is always flat near the center and steep near the peaks (Fig. 12).

For the paraboloid, the results in Fig. 12 show that it is able to produce an almost linear IID curve which is even steeper (on average) than that of the bare transducer.

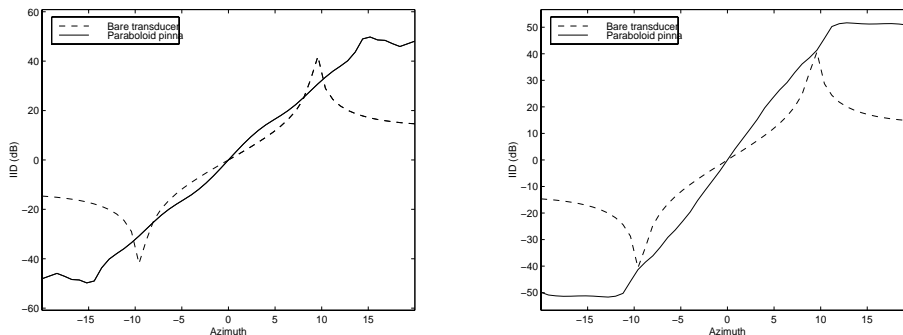


Figure 12: IID performance comparison between paraboloid pinna and bare transducer for the tilting-the-neck (left) and arc scanning (right) experiments.

6.3 Arc scanning

During these experiments, the ears were tilted in a sinusoidal movement with an amplitude of 15° (see Fig. 10). In order to measure the IID, the loudest sound of one complete sweep was taken and for the other ear that sound pressure measured when the ear was at the same position. If the elevation angle of the highest sensitivity of the pinna is independent of the azimuth, always at 0° , this method guarantees that the IID is independent of the target's elevation. For all target elevations the same IID curve over different azimuths is obtained.

For the purpose of comparison between the bare transducer and the transducer with a paraboloid pinna, the results of arc scanning for the bare transducer are shown in the Fig. 13 for a receiver radius of 13 mm and an azimuthal range of 40° .

In part (a) of the figures the directivity of the pinna alone, without the emitter directivity, is shown. If the ears are rotated and not the whole head, the elevation estimation only depends on the pinna and not the emitter directivity. The difference between the main peak and the highest side peak, when arc scanning is performed, is shown in Fig. 13(b).

Sub-plot (e) in the figure shows the elevation for the highest sensitivity. As the bare transducer has an axis of highest sensitivity at 0° elevation (Fig. 13(e)), the IID is independent of the target's elevation (Fig. 13(c)). Wider regions of one grey level correspond

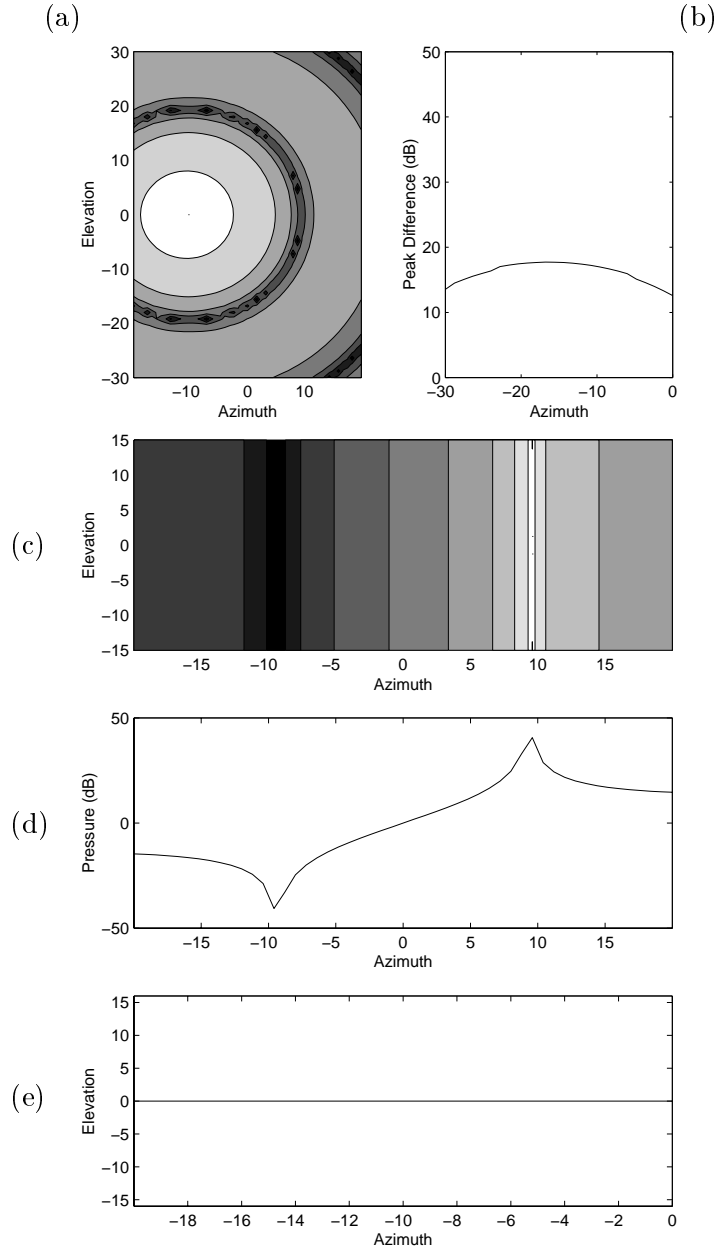


Figure 13: Performance of arc scanning applied to the bare transducer configuration. **Emitter radius of 4 mm and receiver radius of 13 mm.** (a) Directivity of pinna (only receiver). White 3 dB acceptance region. All other regions cover 10 dB. (b) Difference between main and side peak. (c) IID map. (scaling as in (a)). (d) IID curve at 0° elevation. (e) Elevations of maximal amplitude.

to a flatter part of the IID curve (d) and the thinner a region is, the steeper is the IID at that position. The maximal pressure for a bare transducer with the steep IID is -0.47 dB and -23.9 dB for the 4 mm receiver configuration.

Figure 14 shows the results of arc scanning using paraboloid pinnae. Though the steepness of the IID in Fig. 14(d) is on average equal to that of the IID of the bare

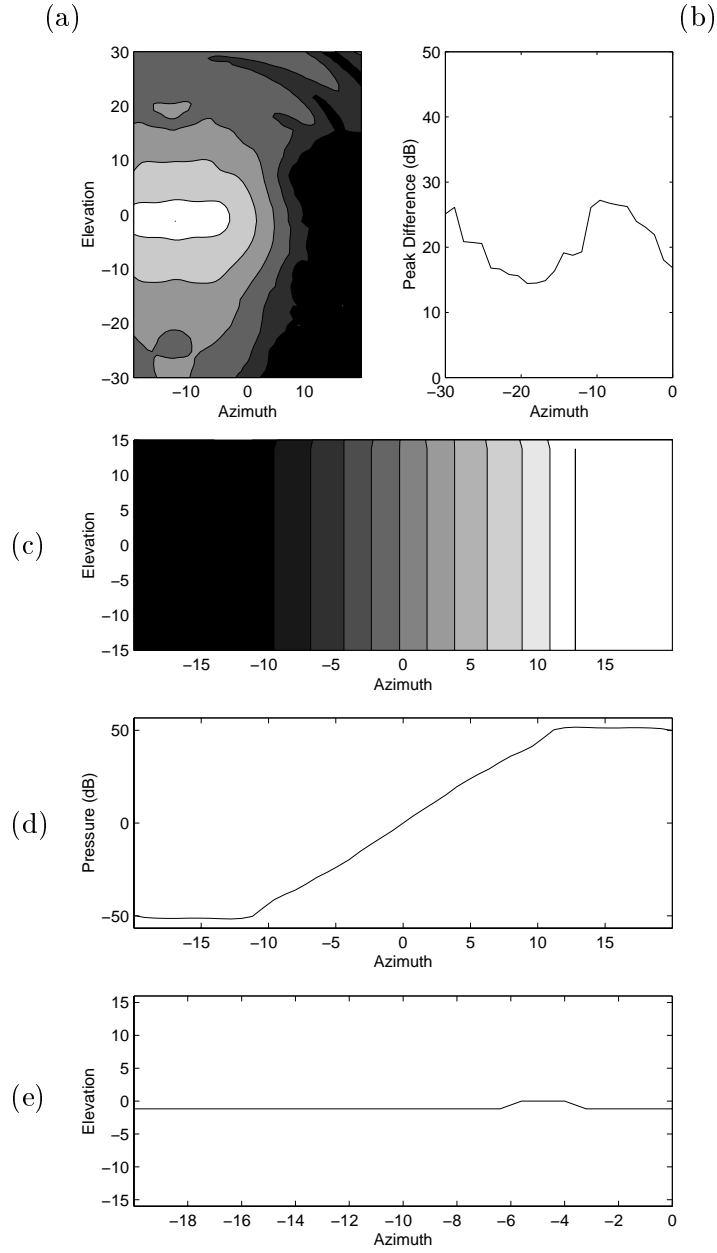


Figure 14: Performance of arc scanning using paraboloid pinnae. **Emitter and receiver radius of 4 mm.** (a) Directivity of pinna (only receiver). White 3 dB acceptance region. All other regions cover 10 dB. (b) Difference between main and side peak. (c) IID map. (scaling as in (a)). (d) IID curve at 0° elevation. (e) Elevations of maximal amplitude.

transducer in Fig. 13(d), it is very linear and therefore much steeper in the center of view (resolution of $0.21^\circ dB^{-1}$ in comparison to $1.1^\circ dB^{-1}$). Due to a slightly irregular maximum sensitivity in elevation (see Fig. 14(e)) the IID map in shows some divergences from the linear pattern for high elevations. The maximal pressure which is received with this pinna shape is -8.9 dB.

Figure 15 is a 3D ray-tracing image of the paraboloid reflector shape mounted on the

sonarhead.

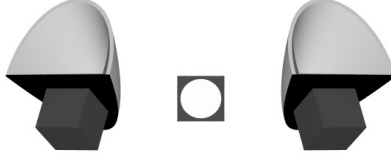


Figure 15: Paraboloid shape which enlarges the range of view to 80° mounted on the sonarhead.

7 Discussion and conclusions

7.1 Improvement with paraboloid pinnae

Comparing the performance of the sonarhead with and without pinnae shows that the paraboloid reflector shapes are able to improve the directivity of the receiver configuration. For both echolocation tasks where the target's elevation is estimated by sweeping the head or only the pinnae, the IID as well as the elevation directivity were enhanced. In contrast to the paraboloid reflectors, the conical exhibited a lower gain and therefore a flatter IID.

- The IIDs of the evolved paraboloid pinnae are steeper, especially in the center of view. The target is more likely to be in the center of view as the bat tries to focus on the target, in order to track it. Therefore, IIDs which are steep for azimuths around 0° are preferable.
- The curvature of the IID could be linearised, which is impossible for the sonarhead without pinnae, if the receiver radius is 13 mm. It is plausible that other shapes of the IID might be evolved which are even steeper in the center of view and flatter in the outer regions.
- The range of view could be increased, without loss of the quality in estimating the target's elevations. Highest IID (HIID) values of up to 48 dB were obtained.

However the IID maps of the evolved shapes exhibit irregularities. The drawback of these uneven IID maps is that the IID depends on the target's elevation. This becomes a problem if the estimation of the target's elevation depends on the estimated azimuth which is obtained by the IID. As this is a recursive dependence, the target localisation becomes impossible. The fitness function used in this study does not consider this problem. In future work the GA should evolve shapes which either have regular IID maps or pinnae which have a constant elevation of maximal sensitivity over all azimuths.

Overall the paraboloid exhibited a flexible behaviour in order to improve different echolocation tasks. However, it is necessary to prove that the results obtained in the simulations coincide with measurements on the reflector shapes mounted on RoBat. One might expect divergences, though their significance is difficult to estimate. Future evolutions should focus more on the assumptions which were made in order to build the acoustic model, especially the limitations due to diffraction.

7.2 Comparison with bat pinnae

The directivity and the resulting IID maps of bats' pinnae are widely investigated. Big differences of the IID maps among the bats make it difficult to compare them to the results of this project. However, some common features were observed.

The model bat *Rhinolophus ferrumequinum* has a HIID (highest IID) of 40 dB, therefore slightly lower than the HIIDs of the paraboloid pinnae of 42 — 55 dB, depending on the IID range. The maximal steepness of the bat's IIDs ($0.6^\circ dB^{-1}$ in one study, in others $0.1^\circ dB^{-1}$ [15]) is comparable to that of the evolved reflectors ($0.21 - 0.8^\circ dB^{-1}$, depending on the scope of view). However the gain of bats' pinnae tend to be much higher (e.g. 24 dB in *Rhinolophus rouxi*). A maximal gain of 21.6 dB with a paraboloid pinna was only achieved if the fitness function had no other optimisation criterium. The gain of evolved shapes which were useful for the echolocation task did not exceed 11.6 dB. This could be caused by an inappropriate acoustic model. Other models approximate the cavity of the bat's pinna with an acoustic horn which has a circular or elliptic entrance [29]. The absolute gain and the changes of gain with frequency for those models coincides well with the observations on bat's pinnae [15].

7.3 Further work

To build and attach real pinnae to the receivers of the sonarhead is the next thing to do. The shape parameters will be taken from the results presented in this work. The real ears will give an insight of how far from reality our simulated work is.

Also, it would be interesting to evolve emitter reflector shapes. These surfaces could focus and direct the sound like the nostrils of *Rhinolophus ferrumequinum* in order to improve together with the pinnae the echolocation task of the biomimetic sonarhead.

Acknowledgments

Jose M. Carmena is supported by the European Union TMR Network SMART2 under contract number FMRX-CT96-0052. Facilities for this work were provided by the University of Edinburgh.

References

- [1] O. Behrend, M. Kössl, and G. Schuller. Binaural influences on Doppler shift compensation of the horseshoe bat *Rhinolophus rouxi*. *J Comp Physiol A*, 185:529–538, 1999.
- [2] C. Biber, S. Ellin, E. Shenk, and J. Stempeck. The Polaroid ultrasonic ranging system. In *67th Convention of the Audio Engineering Society*, New York, October 1980.
- [3] H.J.J. Braddick. *Vibrations, Waves and Diffraction*. McGraw-Hill, London, 1965.
- [4] J.M. Carmena and J.C.T Hallam. Estimating Doppler-shift with a coarse cochlear filterbank. In *Proceedings of the IEEE/RSJ International Conference on Intelligent Robots and Systems (IROS)*, volume 1, pages 221–226, 2000.
- [5] J.M. Carmena, D. Kim, and J.C.T Hallam. Designing artificial ears for animat echolocation. In *From Animals to Animats 6*, Proceedings of the 6th International Conference on Simulation of Adaptive Behaviour, pages 73–80. MIT press, 2000.
- [6] D.R. Griffin, D.C. Dunning, D.A. Cahlander, and F.A. Webster. Correlated orientation sounds and ear movements of horseshoe bats. *Nature*, 196:1185–1186, 1962.

- [7] L. Kay. Air sonars with acoustical display of spatial information. In R.G. Busnel and J.F. Fish, editors, *Animal SONAR Systems (NATO ASI Series)*, pages 769–816. Plenum Press, 1980.
- [8] D. Kim, J.M. Carmena, and J.C.T Hallam. Towards an artificial pinna for a narrow-band biomimetic sonarhead. In *ICES'2000: From Biology to Hardware*, Lecture Notes in Computer Science 1801, pages 113–122. Springer-Verlag, 2000.
- [9] L. Kleeman and R. Kuc. Mobile robot sonar for target localization and classification. *The International Journal of Robotics Research*, 14(4):295–318, 1995.
- [10] J.J. Leonard and H. F. Durrant-Whyte. *Directed Sonar Sensing for Mobile Robot Navigation*. Kluwer Academic Publishers, 1992.
- [11] E.A. Lopez-Poveda and R. Meddis. A physical model of sound diffraction and reflections in the human concha. *J. Acoust. Soc. Amer.*, 100(5):3248–3259, 1996.
- [12] J. Mogdans, J. Ostwald, and H.-U. Schnitzler. The role of pinna movement for the localization of vertical and horizontal wire obstacles in the greater horseshoe bat, *Rhinolophus ferrumequinum*. *J. Acoust. Soc. Amer.*, 84(5):1676–1679, November 1988.
- [13] H. P. Moravec and A. Elfes. High resolution maps from wide angle sonar. In *Proceedings of the IEEE International Conference on Robotics and Automation*, pages 116–121, 1985.
- [14] P. Nachtigall and P. Moore, editors. *Animal SONAR Processes and Performance (NATO ASI Series)*. Plenum Press, 1988.
- [15] M.K. Obrist, M. Brock Fenton, J.L. Eger, and P.A. Schlegel. What ears do for bats: A comparative study of pinna sound pressure transformation in chiroptera. *J. exp. Biol.*, 180:119–152, 1993.
- [16] G. Papadopoulos. Evolving ears for echolocation. Master’s thesis, Department of Artificial Intelligence, University of Edinburgh, 1997.
- [17] H. Peremans, K. Audenaert, and J.M. Van Campenhout. A high-resolution sensor based on tri-aural perception. *IEEE Trans. Robotics and Automation*, 9(1):36–48, February 1993.
- [18] H. Peremans, R. Müller, J.M. Carmena, and J.C.T. Hallam. A biomimetic platform to study perception in bats. In G.T. McKee and P.S. Schenker, editors, *Proceedings of SPIE: Sensor Fusion and Decentralized Control in Robotics Systems III*, volume 4196, pages 168–179, 2000.
- [19] H. Peremans, A. Walker, and J.C.T. Hallam. A biologically inspired sonarhead. Technical Report 44, Dep. of Artificial Intelligence, U. of Edinburgh, 1997.
- [20] H. Peremans, A. Walker, and J.C.T. Hallam. 3D object localisation with a bionic sonarhead: inspirations from biology. In *Proceedings of the 1998 IEEE International Conference on Robotics and Automation*, volume 4, pages 2795–2800, Leuven, Belgium, May 1998.
- [21] H. Peremans, V.A. Walker, G. Papadopoulos, and J.C.T. Hallam. Evolving bat-like pinnae for target localisation by an echolocator. In *Proceedings of the Second International Conference on Evolvable Systems: From Biology to Hardware*, pages 230–239. Springer, 1998.
- [22] J. O. Pickles. *An Introduction to the physiology of hearing*. Academic Press, London, 1982.
- [23] A. Popper and R. Fay, editors. *Hearing by Bats*. Springer Verlag, 1995.
- [24] J.D. Pye and L.H. Roberts. Ear movements in a hipposiderid bat. *Nature*, 225:285–286, 1970.

- [25] H.-U. Schnitzler and A.D. Grinell. Directional sensitivity of echolocation in the horseshoe bat, *Rhinolophus ferrumequinum*. I. directionality of sound emission. *J. Comp. Physiol. A*, 116:51–61, 1977.
- [26] M. Slaney. An efficient implementation of the Patterson-Holdsworth auditory filter bank. Technical Report 35, Apple Computer Inc., 1993.
- [27] Nobuo Suga. Biosonar and neural computation in bats. *Scientific American*, pages 60–68, June 1990.
- [28] B. Tian and H.-U. Schnitzler. Echolocation signals of the greater horseshoe bat (*Rhinolophus ferrumequinum*) in transfer flight and during landing. *J. Acoust. Soc. Am.*, 101(4):2347–64, 1997.
- [29] V. A. Walker. *One tone, two ears, three dimensions: An investigation of qualitative echolocation strategies in synthetic bats and real robots*. PhD thesis, University of Edinburgh, 1997.
- [30] V. A. Walker, H. Peremans, and J. C. T. Hallam. One tone, two ears, three dimensions: A robotic investigation of pinnae movements used by rhinolophid and hipposiderid bats. *J. Acoust. Soc. Amer.*, 104(1):569–579, July 1998.